Fractal Analysis of Virtual Endoscopy Reconstructions

Ronald M. Summers[*] , Lynne M. Pusanik, James D. Malley and Jeffrey M. Hoeg

Diagnostic Radiology Department, Warren Grant Magnuson Clinical Center
National Institutes of Health, Bethesda, MD 20892-1182

ABSTRACT

Virtual endoscopy reconstructions of the body noninvasively provide morphologic information of gross structural abnormalities such as stenoses in airways or blood vessels and polyps in the colonic wall. Surface irregularity or roughness is another indication of abnormality potentially detectible on virtual endoscopy. In this paper, we show how fractal dimension can be used to quantify surface roughness and how these methods may be applied to virtual angioscopy to distinguish the thoracic aorta in a normal volunteer from that of a patient predisposed to atherosclerosis. Finally, we discuss some problems we encountered applying fractal analysis to small, noisy datasets.

Keywords: magnetic resonance angiography; virtual endoscopy; virtual angioscopy; computer-aided diagnosis; vasculature; atherosclerosis; fractal surfaces; three-dimensional reconstruction; homozygous familial hypercholesterolemia

1. INTRODUCTION

Virtual endoscopy is a new method of displaying three-dimensional reconstructions of hollow anatomic structures that simulates conventional endoscopy. In contrast to conventional endoscopy, virtual endoscopy is noninvasive. Virtual endoscopy has been shown to be useful for the assessment of stenoses and masses of the airways [1,2], and for the detection of colonic polyps [3], bladder tumors [4], aneurysms and dissections in blood vessels [5,6]. Virtual endoscopies can be generated by either surface or volume rendering techniques.

The roughness of the wall of a hollow anatomic structure is another abnormality that may be detectible by virtual endoscopy. Roughness of the wall may indicate abnormality of the mucosal or endothelial lining. Examples of wall pathology include inflammation of the bronchial or colonic walls and atherosclerosis of the vasculature. Since roughness of the wall has high frequency, small scale components, roughness can only be detected if there is sufficient resolution in the source images used to generate the virtual endoscopy (e.g., CT or MRI). Current generation CT and MRI scanners are capable of producing images with voxel sizes of 1 mm or smaller which is a prerequisite for measuring roughness.

To date, roughness of the wall has not been clinically useful, in part because of a lack of a way to quantitate it. In this paper, we examine a fractal method of analysis of virtual endoscopy datasets as a measure of surface roughness and use it to quantitate atherosclerosis in virtual angioscopy. Fractals have the property of being self-similar over a wide range of scale and are a natural way to describe roughness. In fact, fractal analysis has been widely applied to images and profiles of surfaces to quantitate their roughness. In medical applications, fractals have been used to quantitate roughness of dental implants[7], orthopedic prostheses[8], and osteoarthritis in joints[9]. Other medical applications of fractals include the measurement of osteoporosis in trabecular bone[10], the detection of tumors in mammograms[11] and histology slides[12], and image compression[13]. Fractal analysis of three-dimensional medical surfaces are less well studied, perhaps due to the complexity of the analysis.

[*] Send correspondence to R.M.S.
E-mail: rms@nih.gov
Web site: http://www.cc.nih.gov/drd

2. METHODS

The fractal dimension (D) is a nonintegral number which lies between the corresponding ideal topological dimension (e.g., D=2 for a surface) and the Euclidean dimension of the space within which the structure is contained (e.g., D=3 for three-dimensional space)[14]. The fractal dimension of a flat surface (a plane) is 2. As a surface becomes more irregular on finer and finer scales, it fills more of the three-dimensional space near itself, and its fractal dimension increases to lie within the range of 2 to 3. When the space near the surface becomes completely filled we have a solid with D=3.

We chose to measure the fractal dimension of virtual endoscopy surfaces by implementing the variation method (See Section 3) [15,16]. The variation method has been shown to produce more stable measures of fractal dimension than the more familiar box-counting method. The method was evaluated on surfaces of known fractal dimension (Takagi surfaces [15] and surfaces produced using the midpoint displacement method with successive random addition [17]) and then used to analyze patient data. See Section 4 for a description of how we implemented the Takagi surfaces.

The method used to generate the midpoint displacement surfaces mathematically simulates fractional Brownian motion which is known to produce a fractal[17,18]. As described in Ref. [14], the algorithm begins with a unit grid, and the corners of the grid are displaced a random distance normal to the grid. The displacement is the product of a given standard deviation (we chose 1.0) and a Gaussian random number. (The random numbers must be chosen carefully; we used the Gaussian random number generator GASDEV[19].) The algorithm then recursively decreases the mesh size and variance of the displacement heights by factors of 2 and $2^{2(3-D)}$, respectively. Finally, at random intervals, all of the points are given random displacements to minimize artifacts.

Virtual angioscopy three-dimensional surface renderings of the thoracic aorta were generated from contrast-enhanced magnetic resonance angiograms (MRA) of a patient with known atherosclerosis and a normal volunteer [20]. The magnetic resonance angiogram images of the thorax were generated using a breathheld oblique sagittal fast spoiled gradient recalled echo three-dimensional pulse sequence applied during the intravenous infusion of a gadolinium contrast agent (Prohance, 0.2 mmol/kg)[21]. The scanning parameters were TR 6.4 ms, TE 1.4 ms with fractional echo, one excitation, 20° flip angle, 28 cm field-of-view, 2 mm slice thickness with 1 mm (50%) overlap, 256x160 matrix and 31.2 kHz readout bandwidth. Zero-filled interpolation was used along all three dimensions[22,23]. Scanning was done under a protocol approved by our Institutional Review Board and written informed consent was obtained.

The images were pre-processed by selecting a volume-of-interest containing the aorta. The signal intensities were scaled down to 8 bits if necessary. A standard isosurface tessellation algorithm was applied and an OpenInventor scene graph of the aorta was produced [24,25]. The surfaces generated with this method can be used for virtual angioscopy. The virtual angioscopies were visualized using a generic virtual endoscopy navigation software tool [26]. Processing and display were done on an Onyx2 Infinite Reality workstation (Silicon Graphics, Inc.) having 1 GB main memory and using a single 195 MHz R10000 processor.

We computed the fractal dimension of the vascular surfaces using the variation method. A representative patch several cm in diameter was cut from each vascular surface using IMEdit software (Innovmetric Software, Québec, CA) and a single fractal dimension was computed for the patch. Each patch was rotated so that the surface normal at the patch center was directed along the z-axis to ensure that the surface is single-valued for each (x,y) pair. If necessary, the patches were also rotated about the z-axis to align the grid of bins with the patch (See Section 3).

3. VARIATION METHOD

Consider a real-valued non-constant function f(x,y) defined on the interval $0 \leq x,y \leq 1$. Following the method of Dubuc [16,27], define the ε-oscillation of the function f in an ε-neighborhood of the point (x,y) as

$$v_f\left(x, y, e\right) = \sup \left| f\left(x_1, y_1\right) - f\left(x_2, y_2\right)\right|, \qquad [1]$$

where the supremum is taken over all data pairs (x_1,y_1), (x_2,y_2) that lie within the grid square (x±ε,y±ε). Next, average v_f over all (x,y) to obtain the ε-variation of f:

$$V_f(e) = \int_0^1 \int_0^1 v_f(x, y, e)\,dxdy \ .$$
[2]

Dubuc has shown that for non-constant functions f(x,y), the fractal dimension D of f is

$$D = \lim_{e \to 0} \left(3 - \frac{\log\ V_f(e)}{\log\ e} \right).$$
[3]

The ε-variation of f is the volume formed by sliding a square of side 2ε along all points of the surface and taking the volume swept out by this square. According to Dubuc, this is an improved version of the so-called Minkowski sausage formed by taking the union of all balls of radius ε centered on the surface. The volume of the Minkowski sausage was used historically to compute the Minkowski-Bouligand dimension and forms the basis of box-counting methods of computing fractal dimension[28].

The implementation of this method for discrete data defined on an N x N grid is as follows. Group the data into R^2 bins, where R<N. The supremum is computed using u(i,j) – b(i,j), where u(i,j) is the maximum value and b(i,j) is the minimum value of the discrete data within the grid squares bounded by the grid indices $(i-k_n, j-k_n)$ and $(i+k_n, j+k_n)$, where $1 \le k_n < R$ and $0 \le i,j < R$. At the boundaries, where $(i-k_n, j-k_n) \le 0$ and $(i+k_n, j+k_n) \ge R$, we choose to mirror the data, e.g., if both i and j exceed R, we use $\sup_n(i,j) = \sup_n(2R-i, 2R-j)$. The size of the grid square (k_n by k_n) relates to the scale $\varepsilon_n = k_n/R$ over which the variation is computed. In this scheme, n = 1, 2, …, n_{max}, where $n_{max} < R$ and k_n are an increasing series of integers (k_n=n is a valid choice). For this discrete data,

$$V_f(e_n) \approx \frac{1}{(R+1)^2} \sum_{i=0}^{R} \sum_{j=0}^{R} \left(u_n(i, j) - b_n(i,j) \right).$$
[4]

The computation is accelerated by computing u_n and b_n from u_{n-1} and b_{n-1} using a pyramid method[15]. This is done by computing the maximum and minimum first on the lines (i) according to

$$u'_n(i, j) = \max(\ u_{n-1}(i-1, j),\ u_{n-1}(i+1, j))$$
$$b'_n(i, j) = \min(\ b_{n-1}(i-1, j),\ b_{n-1}(i+1, j))$$

and then on the columns (j) using

$$u_n(i, j) = \max(\ u'_n(i, j-1),\ u'_n(i, j+1))$$
$$b_n(i, j) = \min(\ b'_n(i, j-1),\ b'_n(i, j+1)) \quad .$$

By swapping the (u_n, b_n) and (u'_n, b'_n) for each iteration of n, memory requirements are kept to a minimum.

The fractal dimension D is the slope of the log-log plot of V_f/ε^3 versus 1/ε. To see that this is true, consider the equation of the line just plotted:

$$\log\ \frac{V_f}{e^3} = D \log\ \frac{1}{e} + c\ ,$$

where c is a constant. Solving for D and expanding, we have

$$D = \frac{c}{\log e} + 3 - \frac{\log V}{\log e}.$$

In the limit as $e \to 0$, this is Equation 3.

This algorithm computes an estimate of the fractal dimension D for each choice of number of bins R. For each value of R, the value of V_f (Equation 4) is computed for a variety of scales (5 – 10 different scales are usually sufficient but must cover a range of scales over several orders of log magnitude). Since there are many possible values of R to choose from, we need a way to determine the optimal bin size (R_{opt}). Dubuc specifies that the best estimate of D is the one where the correlation coefficient of the linear regression fit used to compute the slope of the log-log plot is closest to 1. In practice, only a small number of different bin sizes R are explored since the estimates of D do not vary much for different R and the correlation coefficients are usually all very close to 1.

Experimental data may lie on a regular grid (if they can be evenly sampled) or may be scattered (as with the positions of vertices on a tesselated surface). The analysis of data on a regular grid using the variation method is straightforward and proceeds as described earlier in this section. Scattered data may be handled in two ways. The first method is to sample the surface on a regular grid by determining the height of the surface at each grid location. This method is computationally expensive since ray-surface intersections and interpolations need to be calculated. The second method involves collecting the scattered data into bins and computing the supremum on each bin as for regularly gridded data. This method is extremely fast, especially if the data are appropriately sorted and the bins are large enough so there are at least two datapoints in each bin. For tesselated data such as ours obtained using the marching cubes method[24], the density of the datapoints is usually sufficient if the bins are no smaller than one to two times the original voxel size.

4. TAKAGI SURFACES

The Takagi surfaces are composed of the summation of an elemental shape (the "kernel") whose size and amplitude are varied over a wide range of scales, thereby generating a fractal surface. Although too regular to simulate a naturally occurring rough surface, Takagi surfaces validate the fractal measurement algorithm described in the preceding section.

The equation of a Takagi surface is

$$f(x, y) = \sum_{n=1}^{\infty} b^n \Psi\left(2^{n-1} x, 2^{n-1} y\right), \tag{5}$$

where Ψ is the generating kernel and the constant $b = 2^{D-3}$, $\frac{1}{2} < b < 1$, determines the fractal dimension of $f(x, y)$ [29]. A variety of generating kernels are possible[27]. We have used a pyramidal kernel of the form:

$$x' = x - \text{int}(x), \quad y' = y - \text{int}(y)$$
$$\Psi(x', y') = \min(2x', -2x' + 2, 2y', -2y' + 2)$$

This kernel is similar to that of the Type 1 Takagi function[29].

There are two important implemention issues for the Takagi function. First, one must ensure that x and y are not of the form $i / \left(2^{m-1}\right)$, i and m integers, because Ψ will evaluate to 0 for all n>m. One way to avoid this problem is to add a random offset with sufficient precision (at least 16 digits to the right of the decimal point) to the divisor. Second, the largest evaluable exponent in the arguments to the function Ψ is n=32 using four byte integer arithmetic. One approach to this problem is to observe that only the fractional part of the result is needed. For n=2, compute 2x and keep the fractional part x'. For n=3, use x' just generated and compute $2x'$, and so on.

5. RESULTS

Examples of the Takagi and midpoint displacement surfaces are shown in Figure 1 along with the log-log plots. The computed fractal dimensions for a range of true values are shown in Figure 2. The error on the slope of the log-log plots were typically less than 0.02 units of fractal dimension. To obtain another estimate of the error, we generated three different midpoint displacement surfaces using different sets of Gaussian random deviates. For this experiment, and using a true fractal dimension of 2.5, we found the mean±st. dev. of the computed fractal dimension to be 2.53±0.06.

There was a dramatic difference in processing time between the ray-surface intersection and rebinning methods of implementation of the variation method. For a 256x256 grid, ray-surface intersections required 10 hours of CPU time but rebinning methods required less than 5 minutes.

For the test Takagi surfaces, we were unable to generate results as close to the true values as those reported in Table 2 of Ref. [15]. Our results are closer to those reported in Table 6.5 of Ref. [27]. The log-log plots used to compute the fractal dimension fit well to a straight line (typical Pearson r > 0.999). However, we were unable to reproduce the almost perfect plot of local fractal dimension (a moving average of the fractal dimension taken by computing the regression over limited ranges of the variable k) shown in Figure 6.1 of Ref. [27]. Instead, we found the local fractal dimension to be less than the true value for small k and steadily increasing for larger k.

The effects of smoothing and noise are shown in Figure 3 and Figure 4, respectively. Smoothing tends to reduce the fractal dimension. Noise tends to increase the fractal dimension.

The results for two patient studies are shown in Figure 5. The optimal number of bins were 12 and 16 for the normal subject and patient, respectively. The resolution (density of points) was approximately 30x30. The surface patch of the aorta from the normal volunteer is visibly smoother than that of the patient, and its fractal dimension is lower (2.09±0.05 versus 2.14±0.03). Since D > 2.0, the patches are fractal.

6. DISCUSSION

We have implemented the variation method of fractal dimension determination and confirmed using Takagi and midpoint displacement surfaces that it provides a reasonable measurement of fractal dimension of a surface. We found that, as expected, smoothing a rough surface reduces its fractal dimension and that adding Gaussian noise to a surface increased its fractal dimension. For the virtual angioscopy surfaces, we found that the fractal dimension of the vessel of the normal volunteer was lower (smoother) than that of the patient with atherosclerosis due to hypercholesterolemia. To our knowledge, this is the first demonstration of the application of fractal analysis to virtual endoscopy reconstructions.

Our analysis of the test surfaces showed that the computed fractal dimension deviated from the true fractal dimension. The variation method tends to overestimate the fractal dimension of surfaces with low true fractal dimension and underestimate the fractal dimension of surfaces with high true fractal dimension (Figure 2). This should not be a problem in practice as long as the graph of computed versus true fractal dimension is monotonically increasing. We found this to be the case for the Takagi and midpoint displacement surfaces. If we make the assumption that this is true for virtual endoscopy surfaces also, then within the limits of the error in the value of the computed fractal dimension, one can say that a surface with a lower computed fractal dimension is less rough than a surface with a higher computed fractal dimension.

We found that measured fractal dimensions from midpoint displacement surfaces were closer to the true value than those from Takagi surfaces. This result is reassuring, since the midpoint displacement surfaces appear more similar to the virtual angioscopy surfaces. Possible problems with midpoint displacement surfaces as a test fractal have been proposed relating to the fact that its spectrum is exponential in shape [30].

We were unable to reproduce several of the results in References [15,27]. The reasons for these discrepancies are unclear. There may be subtle differences in implementation of which we are unaware. In one reference, all the necessary experimental parameters were not given (Table 2 of Ref. [15]). Huang et al. has studied some of the limitations of the

variation method and arrived at similar conclusions[31]. Despite these discrepancies, the general trends shown in Figure 2 are similar to those reported previously [27,31].

The fractal dimension computed using the variation method was sensitive to choice of range of scale (k) and varied with the number of bins (R). We used scales from 1 to 50 for 513x513 surfaces but it was not possible to cover as broad a range of scales for the patches of the aorta in which the density of points was much smaller. To compute the fractal dimension accurately, it is generally important to span scales over as wide a range as possible.

The fractal computations of the variation method were relatively time-consuming (approximately 5 min for a 256x256 dataset) because of the required extensive reorganization of the data into bins. The algorithm is $O(N^2)$ [15]. As a practical matter, the computation time becomes a problem when a large number of patches are analyzed, e.g., generation of a map of fractal dimension for an entire virtual endoscopy surface.

The resolution of the dataset can affect the results of the fractal analysis[31]. We found a slight improvement in accuracy when we used a higher resolution (larger N) Takagi dataset. The improvement was very small, however, for the midpoint displacement surfaces. The resolution of the patches of aorta (Figure 5) was much smaller than that of the test datasets, which may in part explain the low fractal dimensions we found for the patches. Analogous to resolution, quantization of data has also been shown to produce lower fractal dimensions[31]. Resolution relates to the density of points in the x-y plane; quantization in a sense relates to the resolution along the z-axis. In our example, the MR angiography datasets were scaled to 8 bits (quantized) before isosurface generation. However, the vertices in the triangular mesh are unquantized floating point numbers, so that the effect of quantization will be complex.

The use of interpolation can also affect the fractal analysis. In this project, we interpolated the MRA dataset (using zero-filled interpolation). For the slower ray-surface intersection method, we also interpolated the surface by sampling it on a regular grid. Depending upon the method used, interpolation would tend to smooth the surface and lower the computed fractal dimension. There exist fractal interpolation methods which could be used to avoid this problem [30].

Quantifying the fractal dimension is a complex problem. For example, the widely used box counting methods are known to be flawed [15,16,30]. Problems with box counting include computation of the slope of a nonlinear log-log plot, and an exquisite sensitivity to the resolution and method of quantization of the data [30]. Other authors have proposed refinements of the box counting method[28]. Our results confirm that the variation method is a relatively robust means of computing fractal dimension for surface patches.

An alternative way to determine the fractal dimension of a blood vessel is to measure the fractal dimension of its profile on one of the MR images (rather than using the virtual angioscopy surface). Fractal analysis of a profile (for example, from an isocontour of a mid-plane oblique sagittal image of the thoracic aorta on a magnetic resonance angiogram) has certain advantages. It is fast (since one only needs to process a single image and processing speed is O(number of bins)) and easier (since one does not need to generate a surface). However, it does not work well if the structure does not fit entirely on one slice (such as evaluation of highly curved or branching structures) or if there is an insufficient density of points on the contour. Nor does it work for the part of the wall that is parallel to the slice, e.g., for the aorta, only the inner and outer edges would be measured. In practice, it is equally difficult to analyze a highly curved virtual endoscopy surface unless the patches can be made small enough and the resolution is adequate to avoid the patch wrapping on itself and becoming multi-valued. However, the surfaces generally contain more points than the profiles and in theory a more accurate fractal dimension could be computed. Both methods (profile and surface) sample a portion of the aorta. In principle, the surface method using patches could be used to determine regional variation of the dimension which may be an advantage.

There are a number of potential sources of error in our fractal analysis. One source is the error in the slope of the log-log plot computed by the regression analysis (typically less than 0.02). Another source of error relates to the rebinning process and the method of selecting the optimal bin size. We estimated this error by computing the fractal dimension for a collection of different midpoint displacement surfaces with the same theoretical fractal dimension and found a standard deviation of D to be 0.06. A more sophisticated error analysis could be done to take into account the error of the computed variation such that weights could be applied to the y-values in the regression analysis of the log-log plot. A method of computing the error in the variation has been proposed for the Takagi surfaces [32]. This method is somewhat difficult to

apply and assumes some knowledge of the true fractal dimension. A more practical approach is to measure the fractal dimension on a number of adjacent surface patches and to use the standard deviation of these measurements as an estimate of the error.

When we added noise to a smooth surface, the computed fractal dimension increased 10% (0.2 units of dimension). Conversely, we found that smoothing the surface decreased the fractal dimension. The effect of noise on quantifying fractal dimension using the variation method has not been extensively studied. In one analysis of the effect of noise on fractal dimension determinations using a variety of methods, it was found that adding only 5% noise (19:1 signal-to-noise ratio) produced as much as a 20% change in measured fractal dimension for the Minkowski method which is similar to the variation method[33]. The MRA datasets we use have signal-to-noise ratios that range from 5 to 20. Therefore, a higher computed fractal dimension could arise from either a truly rough surface or from a noisy dataset. A method of correcting the computed fractal dimension for the effect of noise will need to be determined.

A number of artifacts in medical images can affect the computed fractal dimension in a complex way. Cardiac motion and pulsatility tend to blur the vessel wall, the depiction of the vessel wall in the image representing the average of its position over multiple cardiac cycles. Respiratory motion is another potential artifact[34]. Artifact from temporal or spatial nonuniformity of the concentration of the gadolinium contrast agent within the blood in the vascular lumen over the imaging period[35] could also affect the fractal dimension.

These roughness measures could also be applied to virtual endoscopy systems which only render local anatomy producing endoscopic views based on the small range of structures visible at any one time during endoscopy. Such systems have gained favor because they obviate a difficult segmentation and require less or no pre-processing. For such an application, the vascular surface could be colorized based on its roughness as the physician navigates the particular segment of the hollow anatomic structure. The system would be unable to indicate all potential rough areas up front or to produce an overall measure of roughness because no global 3D anatomic model had been computed.

These methods should work equally well with surface renderings of anatomic surfaces produced from computed tomography scans. The only requirement is that the imaging modality be capable of generating a high resolution three-dimensional model of the surface, with as little noise as possible.

In conclusion, the variation method of fractal analysis provides the physician with a reproducible measurement of roughness of the vessel wall which corresponds with the visual impression of roughness. Fractal analysis may be useful for the serial evaluation of atherosclerosis and for measuring roughness of other anatomic surfaces such as airways, sinuses, urinary tract, biliary tract, and gastrointestinal tract. Image noise is a potential limitation of the technique. We anticipate that future improvements in image acquisition devices expected in the next few years (e.g., multi-ring CT detectors, faster MRI scanners) will provide improved data for use in fractal analysis.

ACKNOWLEDGMENTS

REFERENCES

1. R. M. Summers, D. H. Feng, S. M. Holland, M. C. Sneller and J. H. Shelhamer, "Virtual bronchoscopy: segmentation method for real-time display," *Radiology* **200**, pp. 857-62, 1996.
2. R. M. Summers, W. S. Selbie, J. D. Malley, L. M. Pusanik, A. J. Dwyer, N. A. Courcoutsakis, D. J. Shaw, D. E. Kleiner, M. C. Sneller, C. A. Langford, S. M. Holland and J. H. Shelhamer, "Polypoid lesions of airways: early experience with computer-assisted detection by using virtual bronchoscopy and surface curvature," *Radiology* **208**, pp. 331-7, 1998.
3. A. K. Hara, C. D. Johnson, J. E. Reed, D. A. Ahlquist, H. Nelson, R. L. MacCarty, W. S. Harmsen and D. M. Ilstrup, "Detection of colorectal polyps with CT colography: initial assessment of sensitivity and specificity," *Radiology* **205**, pp. 59-65, 1997.

4. D. J. Vining, R. J. Zagoria, K. Liu and D. Stelts, "CT cystoscopy: an innovation in bladder imaging," *Ajr Am J Roentgenol* **166**, pp. 409-10, 1996.

5. C. P. Davis, M. E. Ladd, B. J. Romanowski, S. Wildermuth, J. F. Knoplioch and J. F. Debatin, "Human aorta: preliminary results with virtual endoscopy based on three- dimensional MR imaging data sets," *Radiology* **199**, pp. 37-40, 1996.

6. F. Kimura, Y. Shen, S. Date, S. Azemoto and T. Mochizuki, "Thoracic aortic aneurysm and aortic dissection: New endoscopic mode for three-dimensional CT display of aorta," *Radiology* **198**, pp. 573-578, 1996.

7. Y. Oshida, A. Hashem, T. Nishihara and M. V. Yapchulay, "Fractal dimension analysis of mandibular bones: toward a morphological compatibility of implants," *Biomed Mater Eng* **4**, pp. 397-407, 1994.

8. G. W. Stachowiak, G. B. Stachowiak and P. Campbell, "Application of numerical descriptors to the characterization of wear particles obtained from joint replacements," *Proc Inst Mech Eng [H]* **211**, pp. 1-10, 1997.

9. N. L. Fazzalari and I. H. Parkinson, "Fractal properties of subchondral cancellous bone in severe osteoarthritis of the hip," *J Bone Miner Res* **12**, pp. 632-40, 1997.

10. S. Majumdar, H. K. Genant, S. Grampp, D. C. Newitt, V. H. Truong, J. C. Lin and A. Mathur, "Correlation of trabecular bone structure with age, bone mineral density, and osteoporotic status: in vivo studies in the distal radius using high resolution magnetic resonance imaging," *J Bone Miner Res* **12**, pp. 111-8, 1997.

11. S. Pohlman, K. A. Powell, N. A. Obuchowski, W. A. Chilcote and S. Grundfest-Broniatowski, "Quantitative classification of breast tumors in digitized mammograms [see comments]," *Med Phys* **23**, pp. 1337-45, 1996.

12. H. Sanders and J. Crocker, "A simple technique for the measurement of fractal dimensions in histopathological specimens," *J Pathol* **169**, pp. 383-5, 1993.

13. J. Ricke, P. Maass, E. Lopez Hanninen, T. Liebig, H. Amthauer, C. Stroszczynski, W. Schauer, T. Boskamp and M. Wolf, "Wavelet versus JPEG (joint photographic expert group) and fractal compression. Impact on the detection of low-contrast details in computed radiographs," *Invest Radiol* **33**, pp. 456-63, 1998.

14. S. Talibuddin and J. P. Runt, "Reliability Test of Popular Fractal Techniques Applied to Small 2-Dimensional Self-Affine Data Sets," *Journal of Applied Physics* **76**, pp. 5070-5078, 1994.

15. B. Dubuc, S. W. Zucker, C. Tricot, J. F. Quiniou and D. Wehbi, "Evaluating the fractal dimension of surfaces," *Proc R Soc Lond A* **425**, pp. 113-127, 1989.

16. B. Dubuc, J. F. Quiniou, C. Roques-Carmes, C. Tricot and S. W. Zucker, "Evaluating the fractal dimension of profiles," *Phys Rev A* **39**, pp. 1500-1512, 1989.

17. D. Saupe In *The science of fractal images*; M. F. Barnsley, R. L. Devaney, B. B. Mandelbrot, H.-O. Peitgen, D. Saupe and R. F. Voss, Ed.; Springer-Verlag: New York, 1988.

18. B. B. Mandelbrot, *The fractal geometry of nature*, W.H. Freeman, San Francisco, 1982.

19. W. H. Press, B. P. Flannery, S. A. Teukolsky and W. T. Vetterling, *Numerical recipes : the art of scientific computing*, Cambridge University Press, Cambridge [Cambridgeshire] ; New York, 1986.

20. R. M. Summers, J. Andrasko-Bourgeois, I. M. Feuerstein, S. C. Hill, E. C. Jones, M. K. Busse, B. Wise, K. E. Bove, B. A. Rishforth, E. Tucker, T. L. Spray and J. M. Hoeg, "The Evaluation of the Aortic Root by MRI: Insights from Patients with Homozygous Familial Hypercholesterolemia," *Circulation* **98**, pp. 509-518, 1998.

21. M. R. Prince, "Contrast-enhanced MR angiography: theory and optimization," *Magn Reson Imaging Clin N Am* **6**, pp. 257-67, 1998.

22. N. M. Hylton, I. Simovsky, A. J. Li and J. D. Hale, "Impact of section doubling on MR angiography," *Radiology* **185**, pp. 899-902, 1992.

23. Y. P. Du, D. L. Parker, W. L. Davis and G. Cao, "Reduction of partial-volume artifacts with zero-filled interpolation in three-dimensional MR angiography," *J Magn Reson Imaging* **4**, pp. 733-41, 1994.

24. W. E. Lorensen and H. E. Cline, "Marching Cubes: A High Resolution 3D Surface Reconstruction Algorithm," *ACM Computer Graphics* **21**, pp. 163-169, 1987.

25. J. Wernecke, *The inventor mentor: Programming object oriented 3D graphics with Open Inventor, release 2*, Addison-Wesley, Reading, Mass., 1994.

26. R. M. Summers, "Navigational aids for real-time virtual bronchoscopy," *AJR Am J Roentgenol* **168**, pp. 1165-70, 1997.

27. B. Dubuc M. Eng. Thesis, McGill University, 1988.

28. C. C. Taylor and S. J. Taylor, "Estimating the Dimension of a Fractal," *Journal of the Royal Statistical Society Series B- Methodological* **53**, pp. 353-364, 1991.

29. B. Dubuc, "On Takagi Fractal Surfaces," *Canadian Mathematical Bulletin-Bulletin Canadien De Mathematiques* **32**, pp. 377-384, 1989.

30. A. I. Penn and M. H. Loew, "Estimating fractal dimension with fractal interpolation function models," *IEEE Transactions On Medical Imaging* **16**, pp. 930-937, 1997.

31. Q. Huang, J. R. Lorch and R. C. Dubes, "Can the Fractal Dimension of Images Be Measured," *Pattern Recognition* **27**, pp. 339-349, 1994.

32. B. Dubuc and S. Dubuc, "Error bounds on the estimation of fractal dimension," *Siam Journal On Numerical Analysis* **33**, pp. 602-626, 1996.

33. J. C. Russ, "Effects of Noise and Anisotropy On the Determination of Fractal Dimensions," *Journal of Microscopy-Oxford* **172**, pp. 239-248, 1993.

34. J. H. Maki, T. L. Chenevert and M. R. Prince, "The effects of incomplete breath-holding on 3D MR image quality," *J Magn Reson Imaging* **7**, pp. 1132-9, 1997.

35. J. H. Maki, M. R. Prince, F. J. Londy and T. L. Chenevert, "The effects of time varying intravascular signal intensity and k-space acquisition order on three-dimensional MR angiography image quality," *J Magn Reson Imaging* **6**, pp. 642-51, 1996.

36. G. Taubin, "A signal processing approach to fair surface design," *SIGGRAPH* pp. 351-358, ACM, Los Angeles, CA, 1995.
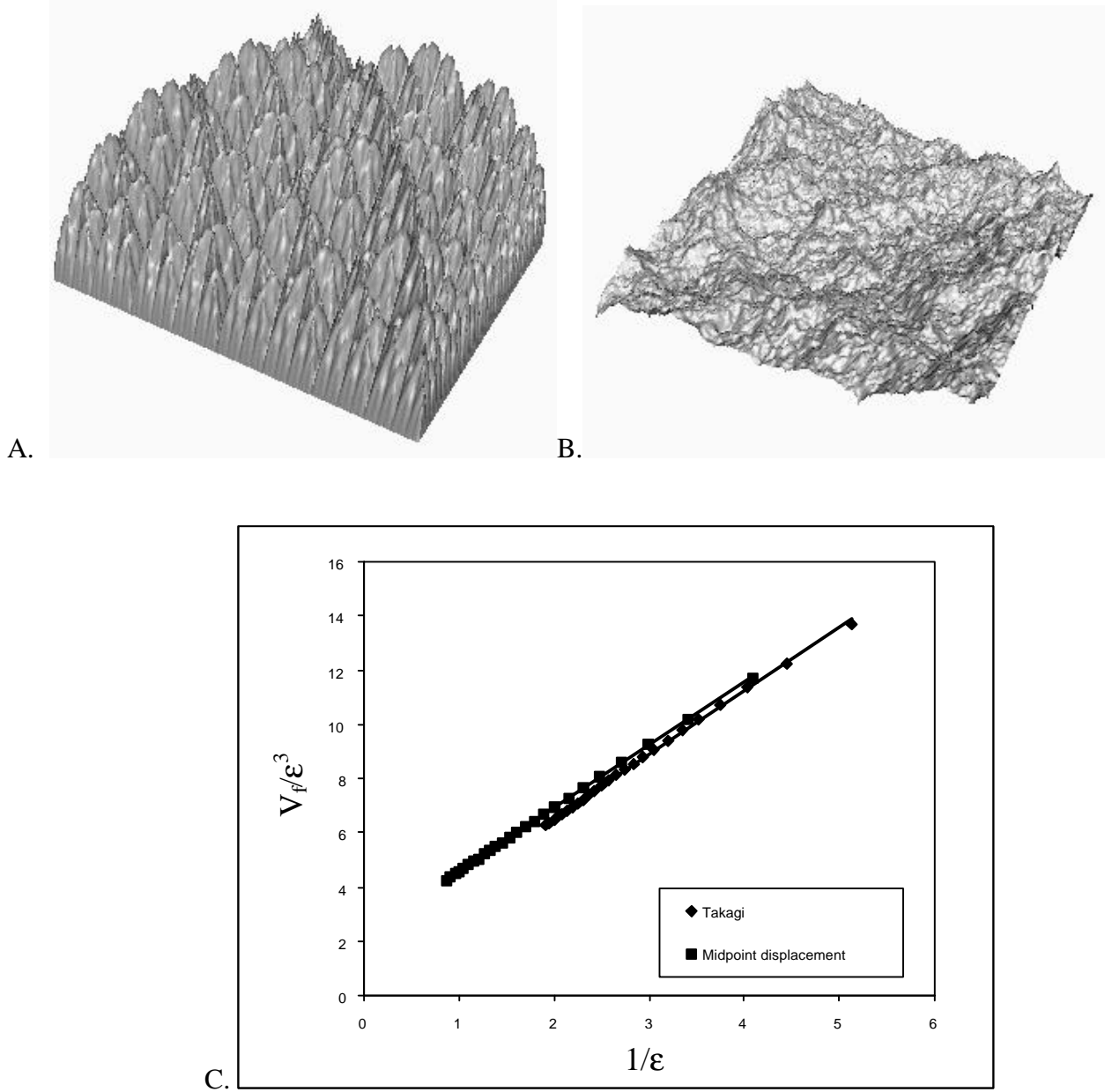
Figure 1. Fractal surfaces used for validation. A. Takagi surface with D = 2.3. B. Midpoint displacement surface with D = 2.3. C. Log-log plots for both surfaces. The computed fractal dimension was 2.34 for the Takagi and 2.33 for the midpoint displacement surfaces. Optimal bin sizes (R_{opt}) were 170 and 60, respectively. Matrix size was 256x256. Takagi surface has a regular, less natural appearance than midpoint displacement surface. Variation method is insensitive to apparent height difference (z-axis scaling) between surfaces in (A) and (B). Differences in scale may provide an illusory impression of roughness compared to more objective fractal analysis. Midpoint data shifted upward slightly to separate two curves in (C).
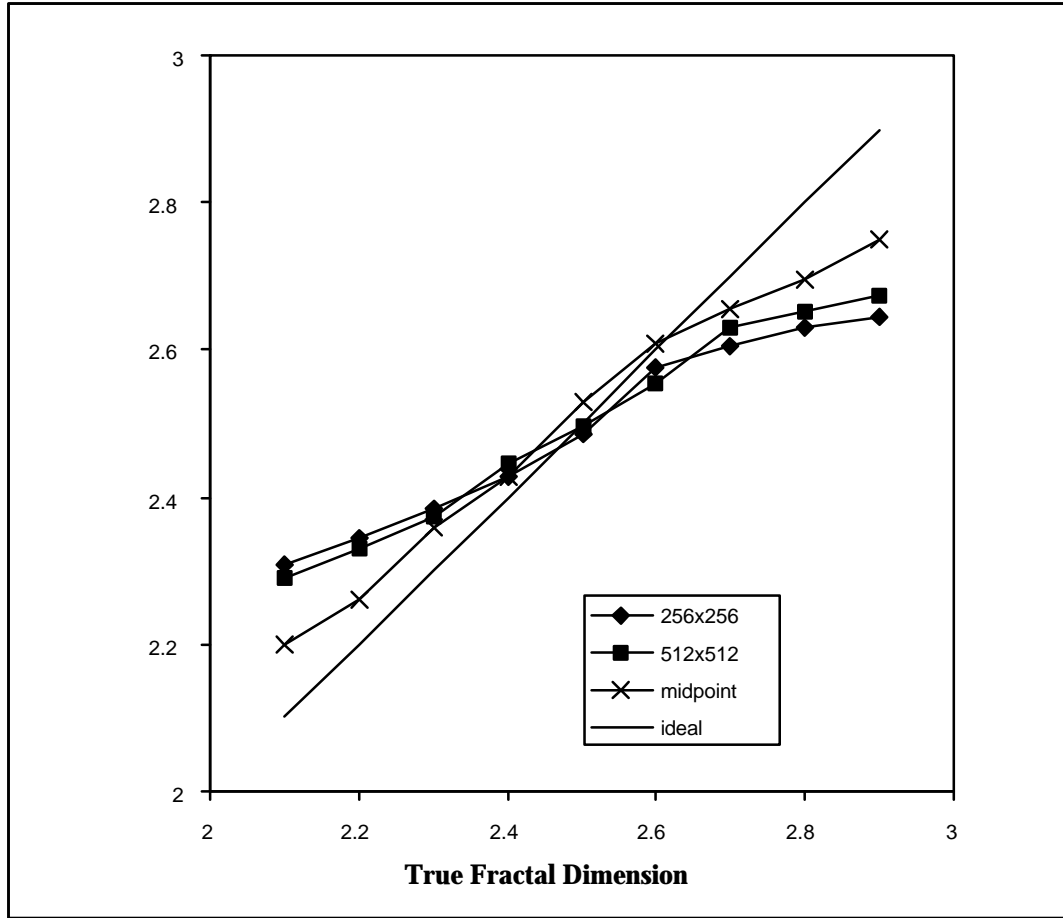
Figure 2. Plot of computed fractal dimension for Type 1 Takagi and midpoint displacement fractal surfaces of known fractal dimension ranging from 2.0 to 2.9. The grid sizes of Type 1 Takagi surfaces were 256x256 (♦) and 512x512 (■) and of midpoint displacement surface (x) was 513x513. Results for a midpoint displacement surface with 257x257 grid were almost identical to that of the 513x513 grid and are omitted for clarity. The Type 1 Takagi kernel was a pyramid on the unit square. Typical uncertainty in computed fractal dimension was ≤ 0.02 units. Line of identity is shown. Note that computed fractal dimension of surfaces with low true fractal dimension (<2.5) is overestimated and of surfaces with high true fractal dimension (>2.5) is underestimated. Since there is a monotonic increase in computed fractal dimension, it is possible to compare the relative fractal dimensions of two surfaces. Note that estimates of the fractal dimension are slightly closer to ideal as the matrix size is increased for the Takagi surfaces. Estimates of the fractal dimension obtained from midpoint displacement surfaces (a more natural appearing rough surface) are closer to the true values compared to those from the Takagi surfaces.
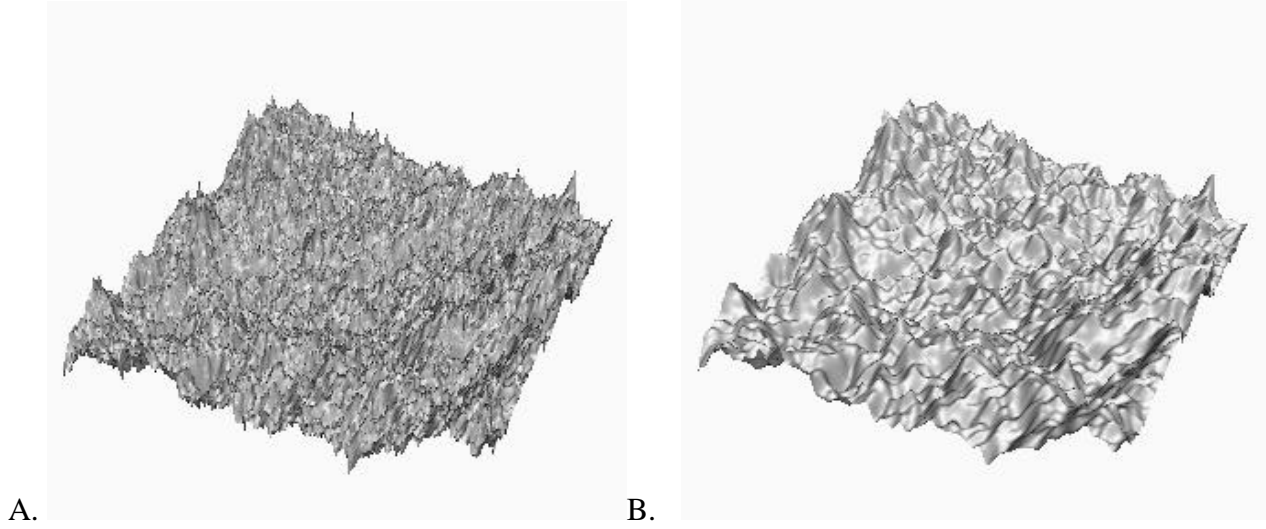
Figure 3. Effect of smoothing on fractal dimension. Midpoint displacement surface with D = 2.5 is shown both before (A) and after (B) 50 iterations of smoothing[36]. The computed fractal dimension of the surface in (A) was 2.48 and in (B) was 2.41. Optimal bin sizes (R_{opt}) were 50 and 45, respectively. Resolution (matrix size) was 256x256.
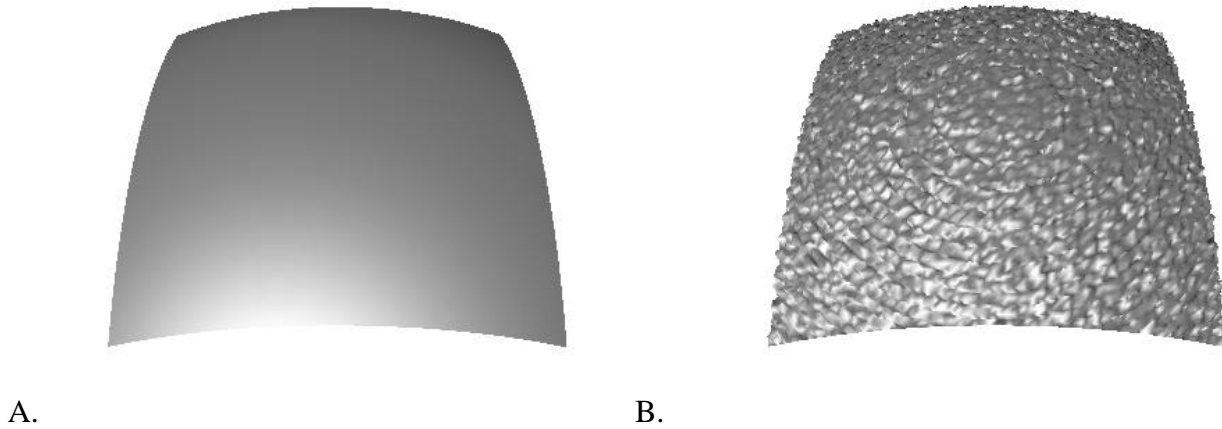

Figure 4. Effect of noise on fractal dimension. A. Segment of a sphere formed by taking an isosurface from a 3D dataset where each voxel value was computed from $x^2 + y^2 + z^2$. B. Segment of a sphere taken after Gaussian noise was added to the 3D dataset. Amplitude (variance) of noise was 2% of the radius of the sphere. Computed fractal dimension of smooth surface (A) was 2.01±0.02 and of noisy surface (B) was 2.21±0.01. Resolution (matrix size) was 100x100. Optimal bin sizes (R_{opt}) were 45 and 75, respectively.
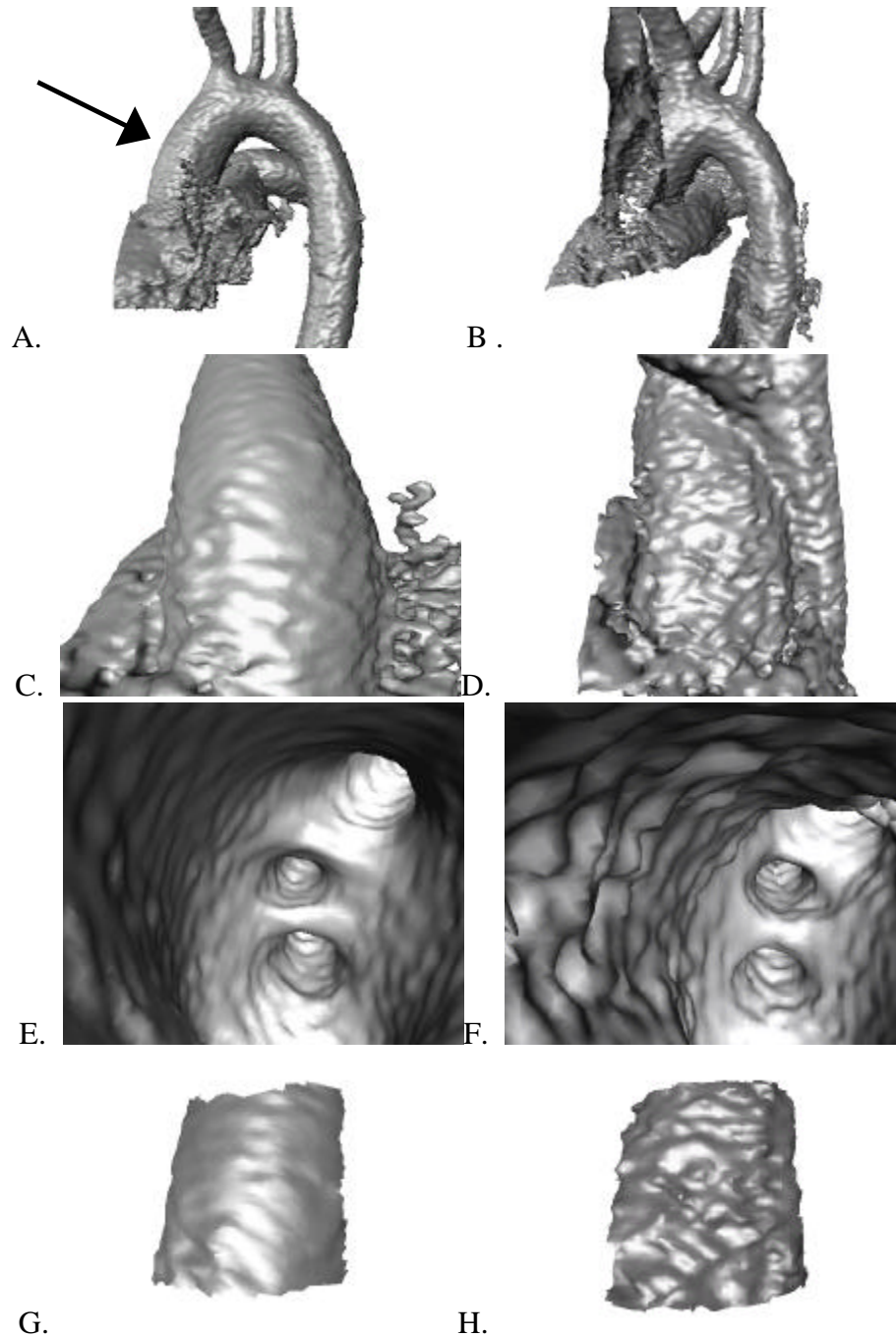
Figure 5. Application of fractal analysis to quantitation of vascular roughness as a measure of atherosclerosis. Three-dimensional shaded surface display of the thoracic aortae of (A, C, E, G) 38 y.o. healthy female subject and of (B, D, F, H) 14 y.o. female patient with homozygous familial hypercholesterolemia. (A, B) Oblique sagittal view of thoracic aorta. (C, D) anteroposterior view of ascending aorta. (E, F) virtual angioscopic view from ascending aorta looking toward arch and origins of great vessels. (G, H) Patch of ascending aorta which was analyzed. Arrow in (A) indicates portion of aorta shown in (C) and (G) and approximate level of viewpoint in (E). The patient had a conventional angiogram one year earlier which showed mild abnormal irregularity of ascending aorta. Virtual angioscopies are from magnetic resonance angiograms obtained following administration of intravenous contrast material and have similar signal-to-noise ratios. The patches are approximately two cm in diameter. The patch from the patient is visibly rougher than that from the normal subject. Fractal dimension of patch of normal subject was 2.09±0.05 and of patient was 2.14±0.03.